Proceedings of the XXI International Conference on Atomic Physics

PUSHING THE FRONTIERS OF ATOMIC PHYSICS

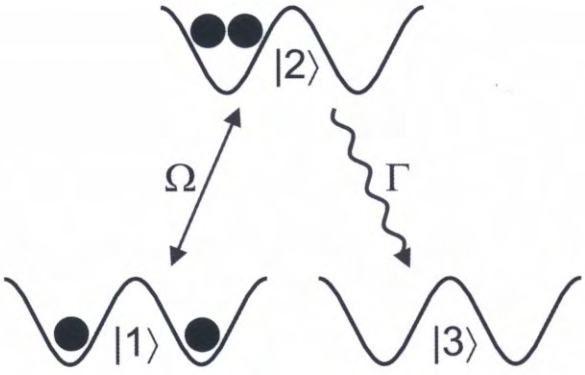

Robin Côté, Phillip L Gould,
Michael Rozman & Winthrop W Smith

editors

World Scientific

Published by

World Scientific Publishing Co. Pte. Ltd.

5 Toh Tuck Link, Singapore 596224

USA office: 27 Warren Street, Suite 401-402, Hackensack, NJ 07601

UK office: 57 Shelton Street, Covent Garden, London WC2H 9HE

British Library Cataloguing-in-Publication Data
A catalogue record for this book is available from the British Library.

PUSHING THE FRONTIERS OF ATOMIC PHYSICS
Proceedings of the XXI International Conference on Atomic Physics

ISBN-13 978-981-4271-99-8
ISBN-10 981-4271-99-3

Printed in Singapore.

MORE ACCURATE MEASUREMENT OF THE ELECTRON MAGNETIC MOMENT AND THE FINE STRUCTURE CONSTANT

D. HANNEKE, S. FOGWELL, N. GUISE, J. DORR and G. GABRIELSE

Department of Physics, Harvard University,
Cambridge, MA 02138, USA

A measurement reported in 2008 uses a one-electron quantum cyclotron to determine the electron magnetic moment in Bohr magnetons, $g/2 = 1.001\,159\,652\,180\,73\,(28)$ [0.28 ppt], with an uncertainty 2.7 and 15 times smaller than for previous measurements in 2006 and 1987. The electron is used as a magnetometer to allow lineshape statistics to accumulate, and its spontaneous emission rate determines the correction for its interaction with a cylindrical trap cavity. The new measurement and QED theory determine the fine structure constant, with $\alpha^{-1} = 137.035\,999\,084\,(51)$ [0.37 ppb], and an uncertainty 20 times smaller than for any independent determination of α.

Keywords: Electron magnetic moment, electron g value, fine structure constant, quantum cyclotron.

1. New Measurement of the Electron $g/2$

A 2008 measurement[1] of the electron magnetic moment $\boldsymbol{\mu}$ determines $g/2$, which is the magnitude of $\boldsymbol{\mu}$ scaled by the Bohr magneton, $\mu_B = e\hbar/(2m)$. For an eigenstate of spin $\mathbf{S}$,

$$\boldsymbol{\mu} = -\frac{g}{2}\,\mu_B\,\frac{\mathbf{S}}{\hbar/2}. \tag{1}$$

This is one of the few measurable properties of one of the simplest of elementary particles – quantifying its interaction with the fluctuating QED vacuum, and probing for electron size or composite structure that has not yet been detected. For a point electron in the simplest renormalizable Dirac description, $g/2 = 1$. QED predicts that vacuum fluctuations and polarization slightly increase this value. Physics beyond the standard model of particle physics could make $g/2$ deviate from the Dirac/QED prediction, as internal quark-gluon substructure does for a proton.

The 1987 measurement that provided the accepted $g/2$ for nearly 20 years[2] was superceded in 2006 by a measurement that used a one-electron quantum cyclotron.[3] Key elements that made the measurement possible included quantum jump spectroscopy and quantum non-demolition (QND) measurements of the lowest cyclotron and spin levels,[4] a cylindrical Penning trap cavity[5] (Fig. 2(a)), inhibited spontaneous emission,[6] and a one-particle self-excited oscillator (SEO).[7] The 2008 measurement[1] has an uncertainty that is 2.7 and 15 times lower than the 2006 and 1987 measurements, respectively, and confirms a 1.8 standard deviation shift from the 1987 value (Fig. 1(a)).

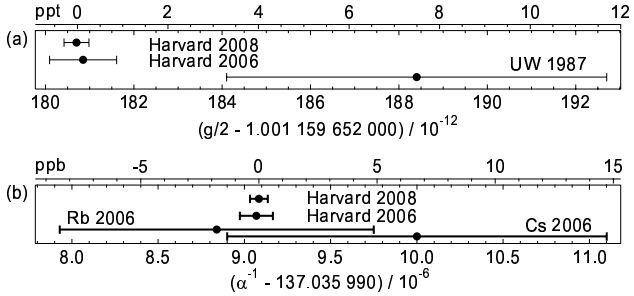

Fig. 1. (a) Most accurate measurements of the electron $g/2$, and (b) most accurate determinations of α.

2. Most Accurate Determination of α

The fine structure constant, $\alpha = e^2/(4\pi\epsilon_0\hbar c)$, is the fundamental measure of the strength of the electromagnetic interaction in the low energy limit. The fine structure constant is also a crucial ingredient of our system of fundamental constants.[8]

The new measurement of the electron $g/2$, with the help of recently updated QED theory,[9] determines α with an uncertainty nearly 20 times smaller than does any independent method (Fig. 1(b)). The uncertainty in α is now limited a bit more by the need for a higher-order QED calculation (underway[9]) than by the measurement uncertainty in $g/2$.

The standard model relates g and α by

$$\frac{g}{2} = 1 + C_2\left(\frac{\alpha}{\pi}\right) + C_4\left(\frac{\alpha}{\pi}\right)^2 + C_6\left(\frac{\alpha}{\pi}\right)^3 + C_8\left(\frac{\alpha}{\pi}\right)^4 + C_{10}\left(\frac{\alpha}{\pi}\right)^5 + ... + a_{\mu\tau} + a_{\text{hadronic}} + a_{\text{weak}}, \quad (1)$$

with the asymptotic series and $a_{\mu\tau}$ coming from QED. Unambiguously prescribed QED calculations (recently summarized[10]) give exact C_2, C_4 and C_6 (all checked numerically), along with a numerical value and uncertainty for C_8, and a small $a_{\mu\tau}$. Very small hadronic and weak contributions are included, along with the assumption that there is no significant modification from electron substructure or other physics beyond the standard model.

The fine structure constant is determined by solving Eq. 1 for α in terms of the measured electron $g/2$:

$$\begin{aligned} \alpha^{-1} &= 137.035\,999\,084\,(33)\,(39) \quad [0.24\text{ ppb}]\,[0.28\text{ ppb}], \\ &= 137.035\,999\,084\,(51) \qquad\quad [0.37\text{ ppb}]. \end{aligned} \tag{2}$$

The first line shows experimental (first) and theoretical (second) uncertainties that are nearly the same. The theory uncertainty contribution to α is divided as (12) and (37) for C_8 and C_{10}. It should decrease when a calculation underway[9] replaces the crude estimate $C_{10} = 0.0\,(4.6)$.[8,10] The α^{-1} of Eq. 2 will then shift by $2\alpha^3\pi^{-4}C_{10}$, which is $8.0\,C_{10} \times 10^{-9}$. A small change Δ_8 in the calculated $C_8 = -1.9144\,(35)$ would add $2\alpha^2\pi^{-3}\Delta_8$.

The total 0.37 ppb uncertainty in α is nearly 20 times smaller than for the next most precise independent methods (Fig. 1(b)). These so-called atom recoil methods[11,12] utilize measurements of transition frequencies and mass ratios, as well as either a Rb recoil velocity (in an optical lattice) or a Cs recoil velocity (in an atom interferometer). (A report in these proceedings may slightly decrease the reported uncertainty in the Rb measurement.)

3. Other Applications of the New Measurement

The accuracy of the new $g/2$ sets the stage for an improved CPT test with leptons. With a one-positron quantum cyclotron we hope to measure the positron g/2 at the same level of accuracy as we did for the electron. The goal is a CPT test with leptons that is much more than an order of magnitude more precise than any other.

Already the most precise test of QED comes from comparing our measured $g/2$ to what can be calculated using Eq. 1 using α from the atom recoil measurements.[10] The accuracy of the QED test is limited almost entirely by the uncertainties in the atom recoils measurements, and not by the much smaller uncertainties in the measured $g/2$ and the QED theory calculation.

Finally, a report[13] suggests that the the accurately measured electron $g/2$ will make possible the discovery of low-mass dark-matter particles, or

will exclude of this possibility. An improved sensitivity requires the new $g/2$ along with a better independent measurement of α.

4. One Electron Quantum Cyclotron

Fig. 2(b) represents the lowest cyclotron and spin energy levels for an electron weakly confined in a vertical magnetic field $B\hat{\mathbf{z}}$ and an electrostatic quadrupole potential. The latter is produced by biasing the trap electrodes of Fig. 2(a). The measured $g/2$ value is primarily determined by the cyclotron frequency $\bar{f}_c \approx 149$ GHz (blue in Fig. 2(b)) and the measured anomaly frequency $\bar{\nu}_a \approx 173$ MHz (red in Fig. 2(b)),[3]

$$\frac{g}{2} \simeq 1 + \frac{\bar{\nu}_a - \bar{\nu}_z^2/(2\bar{f}_c)}{\bar{f}_c + 3\delta/2 + \bar{\nu}_z^2/(2\bar{f}_c)} + \frac{\Delta g_{cav}}{2}. \tag{1}$$

Small adjustments are needed for the measured axial frequency, $\bar{\nu}_z \approx 200$ MHz, and for the relativistic shift, $\delta/\nu_c \equiv h\nu_c/(mc^2) \approx 10^{-9}$. A cavity shift $\Delta g_{cav}/2$ is the fractional shift of the cyclotron frequency caused by the interaction with radiation modes of the trap cavity. Small terms of higher order in $\bar{\nu}_z/\bar{f}_c$ are neglected. The Brown-Gabrielse invariance theorem[14] has been used to eliminate from Eq. 1 the effect of the lowest order imperfections of a real trap – quadratic distortions of the electrostatic potential and misalignments of the trap electrode axis with $\mathbf{B}$.

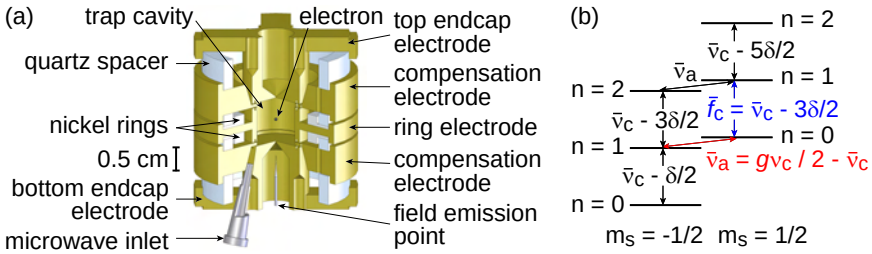

Fig. 2. (a) Cylindrical Penning trap cavity used to confine a single electron and inhibit spontaneous emission, and (b) the cyclotron and spin levels of an electron confined within it.

Quantum jump spectroscopy determines $\bar{f}_c$ and $\bar{\nu}_a$. For each of many trials the system is prepared in the spin-up ground state, $|n = 0, m_s = 1/2\rangle$, after which the preparation drives and detection amplifier are turned off for 1 s. Either a cyclotron drive at a frequency near to $\bar{f}_c$, or an anomaly drive

at frequency near $\bar{\nu}_a$, is then applied for 2 s. The amplifier and a feedback system are turned on to provide QND detection of either a one-quantum cyclotron excitation or a spin flip. Cavity-inhibited spontaneous emission makes the cyclotron excitation persist long enough to allow such detection. The fraction of the excitation trials resulting in excitations is measured.

The cyclotron drive is microwave field injected into the trap cavity through a cold attenuator that keeps black body photons from entering the trap. The anomaly drive is an oscillatory potential applied to electrodes at frequencies near $\bar{\nu}_a$ to drive off-resonant axial motion through the magnetic bottle gradient from two nickel rings (Fig. 2(a)). The electron, radially distributed as a cyclotron energy eigenstate, sees an oscillating magnetic field perpendicular to $\mathbf{B}$ as needed to flip its spin, with a gradient that allows a simultaneous cyclotron transition.[15] To ensure that the electron samples the same magnetic variations while $\bar{\nu}_a$ and $\bar{f}_c$ transitions are driven, both drives are kept on with one detuned slightly so that only the other causes transitions. Low drive strengths keep transition probabilities below 20% to avoid saturation effects.

QND detection of one-quantum changes in the cyclotron and spin energies takes place because the magnetic bottle shifts the oscillation frequency of the self-excited axial oscillation as $\Delta\bar{\nu}_z \approx 4\ (n + m_s)$ Hz. After a cyclotron excitation, cavity-inhibited spontaneous emission provides the time needed to turn on the electronic amplification and feedback, so the SEO can reach an oscillation amplitude at which the shift can be detected.[7] An anomaly transition is followed by a spontaneous decay to the spin-down ground state, $|n = 0, m_s = -1/2\rangle$, and the QND detection reveals the lowered spin energy.

5. Uncertainties and Corrections

Expected asymmetric lineshapes arise from the thermal axial motion of the electron through the magnetic bottle gradient. The axial motion is cooled by a resonant circuit in about 0.2 s to as low as $T_z = 230$ mK (from 5 K) when the detection amplifier is off. For the cyclotron motion these fluctuations are slow enough that the lineshape is essentially a Boltzmann distribution with a width proportional to T_z.[16] For the anomaly resonance, the fluctuations are effectively more rapid, leading to a resonance shifted in proportion to T_z.

The weighted averages of $\bar{\nu}_a$ and $\bar{f}_c$ from the lineshapes determine $g/2$ via Eq. 1. With saturation effects avoided, these pertain to the magnetic field averaged over the thermal motion. It is crucial that any additional

fluctuations in B that are symmetric about a central value will broaden such lineshapes without changing the mean frequency.

To test this weighted mean method we compare maximum likelihood fits to lineshape models. The data fit well to a convolution of a Gaussian resolution function and a thermal-axial-motion lineshape.[16] The broadening may arise from vibrations of the trap and electron through the slightly inhomogeneous field of the external solenoid, or from fluctuations of the solenoid field itself. Because we have not yet identified its source we add a "lineshape" uncertainty based upon the discrepancy (beyond statistical uncertainty) between the $g/2$ values from the mean and fit for the four measurements. To be cautious we take the minimum discrepancy as a correlated uncertainty, and then add the rest as an uncorrelated uncertainty. An additional probe of the broadening comes from slowly increasing the microwave frequency until a one-quantum cyclotron excitation is seen. The distribution of excitations is consistent with the Gaussian resolution functions determined from the fits.

Drifts of B are reduced below 10^{-9}/hr by regulating five He and N_2 pressures in the solenoid and experiment cryostats, and the surrounding air temperature.[3] Remaining slow B drift is corrected based upon lineshapes measured once every three hours. Unlike the one-night-at-a-time analysis used in 2006, all data taken in four narrow ranges of B values (Table 1) are combined, giving a lineshape signal-to-noise that allows the systematic investigation of lineshape uncertainty.

Better measurement and understanding of the electron-cavity interaction removes cavity shifts as a major uncertainty. Cavity shifts are the downside of the cavity-inhibited spontaneous emission which usefully narrows resonance lines and gives the averaging time we need to turn on the SEO and determine the cyclotron state. The shifts arise when the cyclotron oscillator has its frequency pulled by the coupling to nearby radiation modes of the cavity. The cylindrical trap cavity was invented[5] and developed[17] to deliberately modify the density of states of the free space radiation modes in a controllable and understandable way (though not enough to require modified QED calculations[18]). Radiation mode frequencies must still be measured to determine the effective dimensions of a right-circular cylindrical cavity which has been imperfectly machined, which has been slit (so sections of the cavity can be separately biased trap electrodes), and whose dimensions change as the electrodes cool from 300 to 0.1 K.

To the synchronized-electrons method used in 2006, the 2008 measurement also adds a new method – using the electron itself to determine the

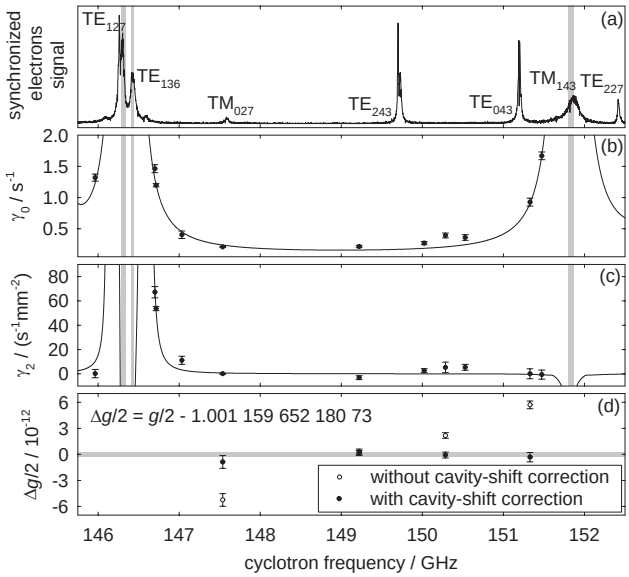

Fig. 3. (a) Modes of the trap cavity are observed with synchronized electrons,[3] as well as (b) with a single electron damping rate γ_0 and (c) its amplitude dependence γ_2. (d) Offset of $g/2$ from our result in Eq. 1 without (open circle) and with (points) cavity-shift corrections, with an uncertainty band for the average.

cavity-electron interaction. The measured spontaneous emission rate for its cyclotron motion, $\gamma = \gamma_0 + \gamma_2 A^2$, depends upon the amplitude A of the axial oscillation through the standing waves of cavity radiation modes. The amplitude is varied by adjusting the SEO,[7] and it is measured by fitting to a cyclotron quantum-jump lineshape.[7,16] Fits of γ_0 and γ_2 (Fig. 3(b)–(c)) to a renormalized calculation of the coupling of the electron and cavity[19] determine the frequencies (with uncertainties represented by the vertical gray bands in Fig. 3(a)–(c)) and Q values of the nearest cavity modes, and the cavity-shift corrections for $g/2$ (Table 1). (Subtleties in applying this calculation to measurements will be reported.) Substantially different cavity-shift corrections bring the four $g/2$ measurements into good agreement (Fig. 3(d)).

6. Results

The measured values, shifts, and uncertainties for the four separate measurements of $g/2$ are in Table 1. The uncertainties are lower for measurements with smaller cavity shifts and smaller linewidths, as might be

Table 1. Measurements and shifts with uncertainties multiplied by 10^{12}. The cavity-shifted "$g/2$ raw" and corrected "$g/2$" are offset from our result in Eq. 1.

$\bar{f}_c$	147.5 GHz	149.2 GHz	150.3 GHz	151.3 GHz
$g/2$ raw	-5.24 (0.39)	0.31 (0.17)	2.17 (0.17)	5.70 (0.24)
Cav. shift	4.36 (0.13)	-0.16 (0.06)	-2.25 (0.07)	-6.02 (0.28)
Lineshape				
correlated	(0.24)	(0.24)	(0.24)	(0.24)
uncorrelated	(0.56)	(0.00)	(0.15)	(0.30)
$g/2$	-0.88 (0.73)	0.15 (0.30)	-0.08 (0.34)	-0.32 (0.53)

expected. Uncertainties for variations of the power of the $\bar{\nu}_a$ and $\bar{f}_c$ drives are estimated to be too small to show up in the table. A weighted average of the four measurements, with uncorrelated and correlated errors combined appropriately, gives the electron magnetic moment in Bohr magnetons,

$$g/2 = 1.001\,159\,652\,180\,73\,(28) \qquad [0.28 \text{ ppt}]. \tag{1}$$

The uncertainty is 2.7 and 15 times smaller than the 2006 and 1987 measurements, and 2300 times smaller than has been achieved for the heavier muon lepton.[20]

Items that warrant further study could lead to a future measurement of $g/2$ to higher precision. First is the broadening of the expected lineshapes which limits the splitting of the resonance lines. Second, a variation in measured axial temperatures, not understood, increases the uncertainty contributed by the wider lineshapes. Third, cavity sideband cooling could cool the axial motion to near its quantum ground state for a more controlled measurement. Fourth, a new apparatus should be much less sensitive to vibration and other variations in the laboratory environment.

7. Self-Excited Proton

The self-excited one-electron oscillator was a crucial ingredient of accurate measurements of the electron $g/2$. Fig. 4 shows one of the first electrical signals detected from a self-excited single proton. Our hope is to improve the sensitivity of this oscillator until non-destructive spin flips of a single trapped proton can be observed as a way to measure g for a proton, and then for an antiproton. If this approach is successful it may be possible to improve the accuracy with which the magnetic moment of the antiproton is measured by a factor of a million or more. An proton/antiproton spin flip is much harder to observe than that of an electron/positron because a nuclear magneton is 2000 times smaller than a Bohr magneton.

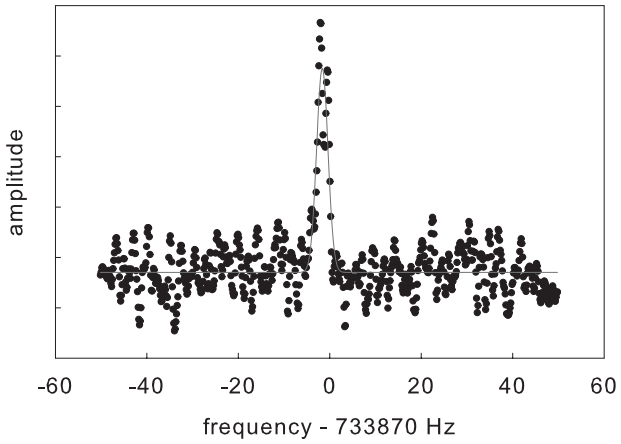

Fig. 4. First example of the signal from a self-excited proton oscillator.

8. Directly Driven Electron Spin Flip

The two electron spin states could potentially be a very high fidelity q-bit. As one small step, Fig. 5 shows the first line shape for a electron driven directly near its spin frequency, rather than at the difference between the spin and cyclotron frequencies.

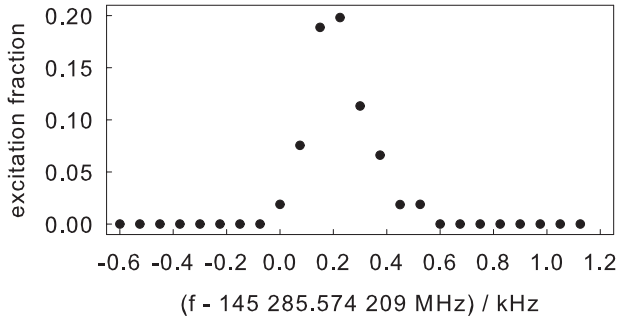

Fig. 5. First example of the lineshape for electron spin flips driven directly at the spin frequency.

9. Conclusion and Acknowledgments

In conclusion, a new measurement of the electron $g/2$ is 15 times more accurate than the 1987 measurement that provided $g/2$ and α for nearly 20

years, and 2.7 times more accurate than the 2006 measurement that superseded it. Achieving the reported electron $g/2$ uncertainty with a positron seems feasible, and would make the most stringent lepton CPT test. With QED and the assumption of no new physics beyond the standard model of particle physics, the new measurement determines α almost 20 times more accurately than any independent method. The measured $g/2$ is accurate enough to allow testing QED, probing for electron size, and searching for a low mass dark matter particle if a more accurate independent measurement of α is realized.

More details are in the thesis of D. Hanneke, and being readied for publication. This work was supported by the NSF AMO program.

References

1. D. Hanneke, S. Fogwell and G. Gabrielse, *Phys. Rev. Lett.* **100**, 120801 (2008).
2. R. S. Van Dyck, Jr., P. B. Schwinberg and H. G. Dehmelt, *Phys. Rev. Lett.* **59**, 26 (1987).
3. B. Odom, D. Hanneke, B. D'Urso and G. Gabrielse, *Phys. Rev. Lett.* **97**, 030801 (2006).
4. S. Peil and G. Gabrielse, *Phys. Rev. Lett.* **83**, 1287 (1999).
5. G. Gabrielse and F. C. MacKintosh, *Intl. J. Mass Spec. Ion Proc.* **57**, 1 (1984).
6. G. Gabrielse and H. Dehmelt, *Phys. Rev. Lett.* **55**, 67 (1985).
7. B. D'Urso, R. Van Handel, B. Odom, D. Hanneke and G. Gabrielse, *Phys. Rev. Lett.* **94**, 113002 (2005).
8. P. J. Mohr and B. N. Taylor, *Rev. Mod. Phys.* **77**, 1 (2005).
9. T. Aoyama, M. Hayakawa, T. Kinoshita and M. Nio, *Phys. Rev. Lett.* **99**, 110406 (2007).
10. G. Gabrielse, D. Hanneke, T. Kinoshita, M. Nio and B. Odom, *Phys. Rev. Lett.* **97**, 030802 (2006), *ibid.* **99**, 039902 (2007).
11. P. Cladé, E. de Mirandes, M. Cadoret, S. Guellati-Khélifa, C. Schwob, F. Nez, L. Julien and F. Biraben, *Phys. Rev. A* **74**, 052109 (2006).
12. V. Gerginov, K. Calkins, C. E. Tanner, J. J. McFerran, S. Diddams, A. Bartels and L. Hollberg, *Phys. Rev. A* **73**, 032504 (2006).
13. C. Boehm and J. Silk, *Phys. Lett. B* **661**, 287 (2008).
14. L. S. Brown and G. Gabrielse, *Phys. Rev. A* **25**, 2423 (1982).
15. F. L. Palmer, *Phys. Rev. A* **47**, 2610 (1993).
16. L. S. Brown, *Ann. Phys. (NY)* **159**, 62 (1985).
17. J. N. Tan and G. Gabrielse, *Appl. Phys. Lett.* **55**, 2144 (1989).
18. D. G. Boulware, L. S. Brown and T. Lee, *Phys. Rev. D* **32**, 729 (1985).
19. L. S. Brown, G. Gabrielse, K. Helmerson and J. Tan, *Phys. Rev. Lett.* **55**, 44 (1985).
20. G. W. Bennett *et al.*, *Phys. Rev. D* **73**, 072003 (2006).